SKR polarization and source localization with the Cassini/RPWS/HFR instrument: First results

B. Cecconi*, P. Zarka†, and W. S. Kurth*

Abstract

The High Frequency Receiver (HFR) of the Radio and Plasma Wave Science experiment (RPWS) experiment has direction-finding (DF) capabilities, i.e. it allows us to retrieve quasi-instantaneously the direction of arrival of an incoming wave, its polarization state and its flux. We use these DF capabilities to characterize the source position and polarization state of the main kronian radio emission: the SKR (Saturnian Kilometric Radiation). We expose a full polarimetric study of the southern SKR sources. We also show the localization of the region of emission which confirms that the northern emission is right-handed and the southern one is left-handed, which is compatible with the Cyclotron-Maser Instability emission process. We also observe a possible O-mode radio emission coming from the southern hemisphere of Saturn.

1 Introduction

Discovered with the Voyager Planetary Radio Astronomy (PRA) experiment by Kaiser et al. [1980], the Saturn's Kilometric Radiation (SKR) is the most intense component of the kronian radio emissions (see reviews by Kaiser et al. [1984], Zarka [1998, 2000]). This nonthermal radio emission covers the frequency range from $\sim$10 *kHz* to 1.2 *MHz* with a peak intensity at about 200 *kHz*. The SKR is sporadic but shows arc-like structures (see Figure 1), although not as organized as at Jupiter. There are several hypothesis for the particle acceleration processes leading to the auroral precipitations [Galopeau et al., 1995; Cowley et al., 2004], but the SKR emission process itself is established to be the Cyclotron Maser instability (CMI) [Louarn, 1992, and references therein]. In–situ measurements within the region of emission of the terrestrial Auroral Kilometric Radiation (AKR) [De Feraudy, 1988] proved the validity of this model. Even though no such in–situ measurement has been carried out at other planets, this emission process is the one that meets the observational constraints for nonthermal planetary radio emissions (such as polarization, brightness temperature, frequency cut-off, beaming and localization) [Zarka,

*Department of Physics an Astronomy, University of Iowa, Iowa City, USA
†LESIA, CNRS–Observatoire de Paris, Meudon, France

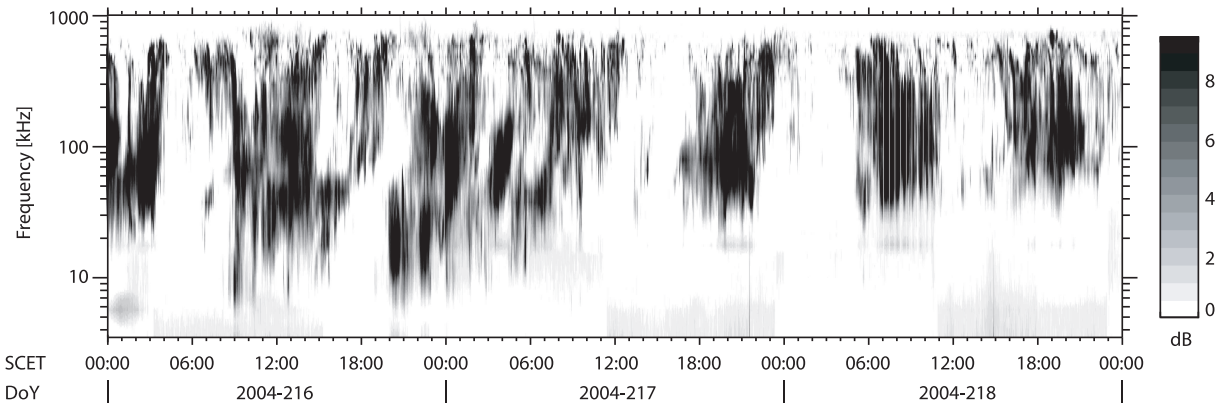

Figure 1: Typical dynamic spectrum showing the kronian radio emissions, days 2004-216 to 218 (Aug. 03–05, 2004) for the whole SKR range. The intensity is represented in dB above background. The SKR radio emissions are present from ∼10 kHz to ∼800 kHz here. As can be seen on this figure, the SKR is very sporadic with some arc-like structure (although less organized than the Jovian auroral radio emissions). The SKR also shows a ∼10.66 hour periodicity (most visible here after 12:00, day 2004-217).

1998]. The SKR polarization characteristics are compatible with the CMI process: the SKR is strongly circularly polarized [Ortega-Molina and Lecacheux, 1990]; it is right–handed (RH) in the northern hemisphere and left–handed (LH) in the southern one, indicating an emission in the extraordinary (X) mode. The polarization results presented in this paper will further consolidate this hypothesis.

The auroral origin of the SKR was proposed since the first observations [Kaiser et al., 1980]. The SKR sources localization has been indirectly inferred from the Voyager PRA data [Galopeau et al., 1995 and previous references as discussed therein] and was found fixed in local time (LT): centered approximately toward noon (12:00LT) at high magnetic latitudes ($\geq 80°$), and extending toward lower latitudes on the morning side (down to 60° at ∼09:00LT). This localization is consistent with the ultraviolet (UV) auroral emission [Gérard et al., 1995; Trauger et al., 1998; Gérard et al., 2004; Kurth et al., 2005a].

Launched in 1997, the Cassini spacecraft arrived at Saturn in July 2004. It is the fourth spacecraft (after Voyager 1 and 2, and Ulysses) including radioastronomy instrumentation that can observe the Saturn's radio emissions. The High Frequency Receiver (HFR) of the Radio and Plasma Wave Science experiment (RPWS) experiment has direction finding (DF) capabilities. This means that we can retrieve the polarization (typically the polarization Stokes parameters: U and Q for linear polarization, V for circular polarization), direction of arrival (typically two angles: the colatitude θ and the azimuth ϕ) and flux (S) of an incoming free–space propagating electromagnetic wave. Moreover, the HFR DF capabilities are quasi instantaneous (10–40 *ms*) contrarily to spinning DF capable spacecrafts like Ulysses or Wind for which at least one rotation of the spacecraft is necessary to obtain DF measurements (12 *s* for Ulysses).

The DF inversion methods we use in this paper are described in Cecconi and Zarka [2005].

As the HFR is most of the time in its dipole mode (where two of its three electrical monopole antennas are connected together and used as a dipole), we will be using only 2-antenna DF in this paper (see Cecconi and Zarka [2005]). In the 2-antenna mode, we get 4 instantaneous measurements: 2 autocorrelation (1 for each antenna) and 1 complex cross-correlation. The DF inversions consist of expressing the 6 wave parameters (S, Q, U, V, θ and ϕ) in terms of our measurements. This implies that for 2-antenna measurements, we will have to make assumptions on at least 2 of the wave parameters. We are going to use two particular inversions : (i) the *polarimeter inversion* where the source position has to be known; (ii) the *circular goniometer inversion* where a no linear polarization assumption (U=Q=0) is made. We use the electrical antenna parameters calibrated by Vogl et al. [2004] during the Cassini-Jupiter flyby.

We will first present SKR polarization results, using data recorded during the Cassini inbound trajectory before the insertion into orbit around Saturn. We will then present SKR localization measurements. Those results will be discussed in the last section.

2 SKR Polarization

The SKR is emitted by the CMI process in the X mode, near the local cyclotron electronic frequency (f_{ce}). Using the magnetic field model given by Connerney et al. [1984], we calculate that the SKR should be emitted within 1.1 to ∼4 R_S (Saturn radii) from the center of Saturn. If we wish to assume that SKR comes from the direction of Saturn and ignore the offset from Saturn's center, Cassini has to be further than ∼175 R_S from the planet. At this distance, a sphere of diameter 3 R_S subtends an angle of less than 1°. This order of magnitude for the acceptable error on the source position has been chosen after the uncertainty on the calibrated electrical antennas, which is of the order of 1–2°. This situation last occurred on day 2004/165 (June 4, 2004). It will never happen again during the primary mission. We will thus use data acquired before this date for the *polarimeter inversion* and assume that the source position is at the position of Saturn. This inversion provides the Stokes parameters.

We used the HFR data from day 2004-002 to 2004-016. Solar or faint possible jovian radio bursts were removed from the data set by hand. Note that in the case of solar bursts which are not polarized, a test on the circular polarization degree would remove them automatically but as we are willing to characterize the SKR polarization, we shall not do any a priori selection on the polarization itself. In addition to this visual SKR data selection, we applied 3 other data selections: (i) signal to noise (SNR) selection which was SNR>20 *dB* on both antennas; (ii) a geometrical selection (as described in Cecconi and Zarka [2005]) α_{xw}>20°, where α_{xw} is the elevation of Saturn above the plane formed by the x dipole and w monopole antennas (see Gurnett et al. [2004]). The analysis has been carried out with three different frequency selections: 0–100 *kHz*, 100–325 *kHz* and 325–1000 *kHz*.

Fig. 2 shows the results for three frequency bands: LF (0–100 *kHz*), MF (100–325 *kHz*) and HF (325–1000 *kHz*) bands. We display histograms of occurrence for circular polarization degree (V, which stands for V Stokes parameter); total linear polarization degree

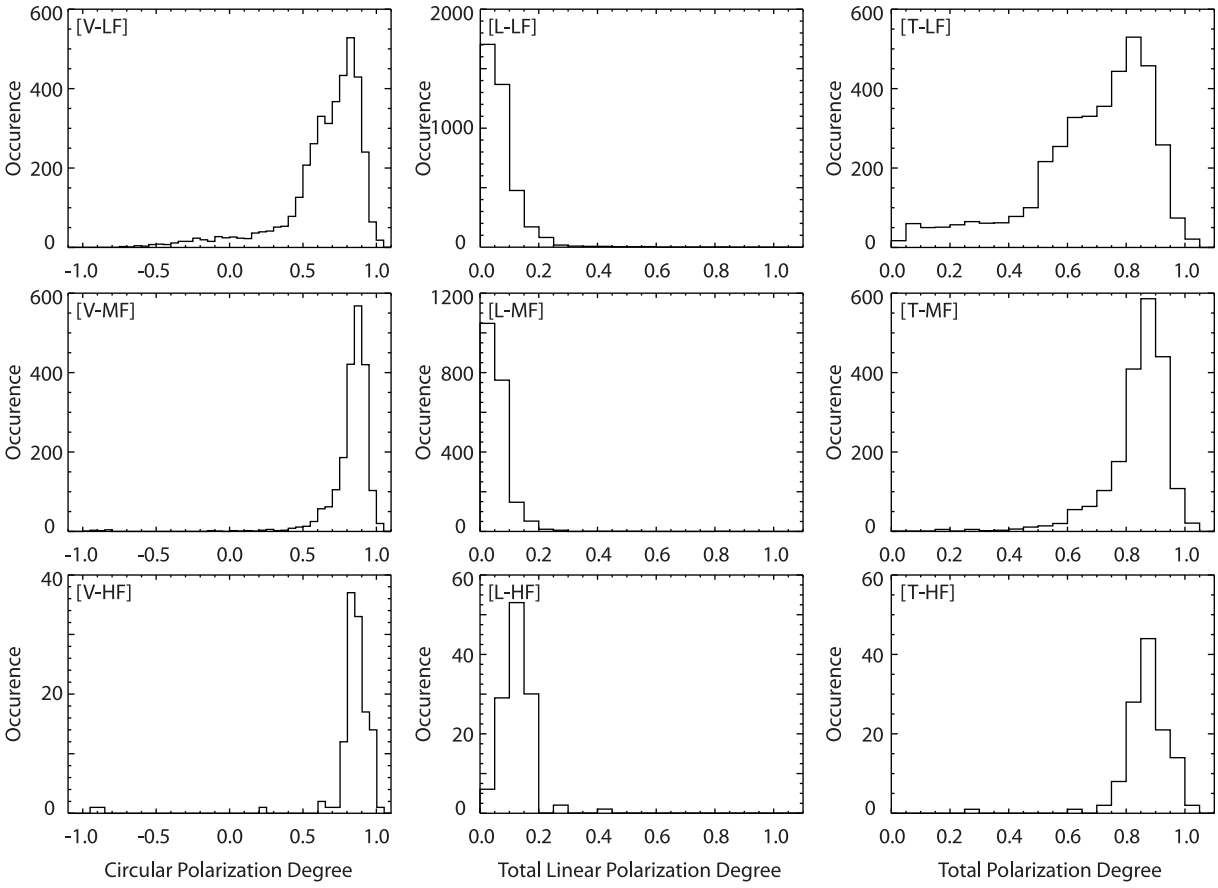

Figure 2: Polarization degree (V for circular, L for linear and T for total polarization degree) histograms for the three frequency band: LF (10–100 kHz), MF (100–325 kHz) and HF (325–1200 kHz). We have used data recorded between days 2004/002 and 2004/016 and computed the polarization degree through the polarimeter inversion, *assuming the source position to be at Saturn. The SKR data has been selected with the following criteria: SNR>20 dB on each antenna; α_{xw}>20°. A total of 3865, 2051 and 121 samples is selected in bands LF, MF and HF respectively. The selected data represent respectively 0.3%, 0.02% and 0.005% of the total data sample for bands LF, MF and HF. Note that a 0.10 linear polarization degree bias appears in HF. It is an artifact due to both interferences lines and the small number of selected data.*

Frequency Band (*kHz*)	total number of measurements	number of selected samples	Total Polarization Degree ($\pm\sigma$)
0–100	2,053,332	3,865	0.76±0.16
100–325	741,578	2,031	0.87±0.07
325–1000	2,199,952	121	0.87±0.06

Table 1: Summary of Polarization measurements. For each frequency band, we show the total number of samples recorded by the HFR, the number of samples selected with the data selection criteria, and the total polarization degree, measured by fitting a gaussian function to the total polarization histograms.

histogram (L, computed from the 2 linear polarization Stokes parameters as $(Q^2+U^2)^{1/2}$); and total polarization degree histogram (T, computed as $(Q^2+U^2+V^2)^{1/2}$). See Table 1 for detailed numerical results.

The effective integration times that were used on the receiver during the period of time selected for the polarization measurement were discussed by Gurnett et al. [2004]. They are the following: ∼220 *ms* from 3.5 to 16 *kHz* (band A), ∼90 *ms* from 16 to 71 *kHz* (band B), ∼26 *ms* from 71 to 319 *kHz* (band C), and for frequencies between 325 and 2000 *kHz* (band H1): 30 *ms* (from day 2004-002 to day 2004-009 12:00) and 15 *ms* (from day 2004-009 12:00 to day 2004-016). In each bands the integration times and bandwidths are chosen in order to have a constant noise level $n = 1/\sqrt{b\tau}$ (with b, the bandwidth and τ the integration time) within the band. Hence, we have $n = 0.072$ (band A), 0.053 (band B), 0.047 (band C) and 0.035 (band H1).

The histogram in Fig. 2[MF] shows that the SKR emissions detected by Cassini are strongly left-handed (LH) as the degree of circular polarization is positive. These observations are in total agreement with Voyager data mentioned earlier as Cassini only sees the southern kronian pole at this time (see Kurth et al. [2005a]). Histogram 2b shows that the SKR has no linear polarization component. The spread of the histogram is due to the uncertainties which are of the order of 0.1 for absolute Stokes parameter determination (see Cecconi and Zarka [2005]). The total polarization degree (Figure 2c) is measured at 87% of polarization with only circular polarization (with a 0.14 full width at half maximum, close to the 0.10 accuracy as shown in Cecconi and Zarka [2005]). Fig. 2[LF] shows that at low frequency, the accuracy on the result is lower. This can be explained in three ways: (i) our assumption that the source is close to Saturn may be wrong as the lower the frequency is, the higher the altitude of the emitting regions is supposed to be; (ii) at low frequencies, the background level is more variable than at higher frequencies — as can be seen on Fig. 1 — depending on the local plasma parameters and thus can lead to erroneous background subtraction; (iii) the intrinsic polarization degree might also be lower at low frequencies. This last point would need a refined analysis on shorter time scales which is beyond the scope of this paper. Fig. 2[HF] (325–1000 *kHz* band) shows a similar histogram as for the 100–325 *kHz* band, except that the linear polarization degree histograms shows a peak at ∼0.10. This is interpreted as an artifact due to both onboard interference lines and the small number of selected data samples.

3 SKR Localization

As for the SKR polarization measurements, the SKR localization results presented here have been obtained using 2-antenna measurements (HFR in dipole mode), but using the *circular goniometer inversion*, assuming that the SKR has no linear polarization (i.e. forcing Q=U=0) and computing S, V, θ and ϕ. We present data recorded in early 2005. The first period we will study is day 2005-040 (Feb. 9, 2005), between 00:00 and 01:00 SCET (spacecraft event time). Cassini was then at ∼49 R_S from Saturn, and at ∼08:00 LT. In this configuration, we will observe the dayside sources from a distant range. The second period we will study is day 2005-089 (March 30, 2005), just after the 7th perikrone which occurred at about 00:00 SCET. Cassini is close to Saturn (5–10 R_S for the presented measurements) and on the night side (01:00–03:30 LT).

3.1 Dayside distant observations (day 2005-040)

The period of time presented in this section was recorded during day 2005-040. We present DF results for the 00:00–01:00 SCET period. The Cassini spacecraft was at ∼49 R_S from Saturn, 3.1° below the equatorial plane and at 08:05 LT. Fig. 3a shows the dynamic spectrum for the 00:00–04:00 SCET period. The two red boxes show the time-frequency selections used to compute the maps on Fig. 3c–e. Fig. 3b shows the circular polarization degree over the same period of time as computed with the *circular goniometer inversion*; white, black and grey areas represent respectively LH, RH and no polarization (or no data selected). The selection applied to the data is given in the caption of Fig. 3. The maps given in Fig. 3c–e are 2D intensity histograms. Each bin represents a solid angle with a 0.5 R_S × 0.5 R_S squared cross-section at the distance of Saturn. This allows us to build time integrated maps, even if the Saturn–Cassini distance is variable over the integration time. The level of each bin shows a weighted sum of the computed intensities S of the selected data, taking into account the real band width and integration time for each selected sample, and the variation of the distance to Saturn. The data selection was made on: (i) SNR>33 *dB* on at least one antenna; (ii) time interval; (iii) frequency band; (iv) polarization degree V (LH polarization maps are computed with V>0.3, RH ones with V<−0.3); (v) and α_{xw}>20°. The SNR and the geometrical threshold values are justified by the desired 1–2° accuracy on the localization results (see Table 2 in [Cecconi and Zarka, 2005]).

The map on Fig. 3c corresponds to an integration on the whole frequency range (10–1000 *kHz*) between 00:00 and 01:00 SCET, and selecting for LH polarization (V>0.3). The source is seen on the southern hemisphere on the noon side. The map on Fig. 3d corresponds the low frequency (f<60 kHz) emission seen on Fig. 3a between 00:00 and 01:00 SCET. We selected RH radio emission (V<−0.3) and we observe that the source is detected in southern hemisphere on the noon side. At higher frequency (f>60 kHz), for the same period of time (see map on Fig. 3e), the source is detected in the northern hemisphere on the noon side. In each case, the sources are approximately at 2–3R_S from the center of Saturn.

Figure 3d then shows an example of a possible southern RH source which corresponds to

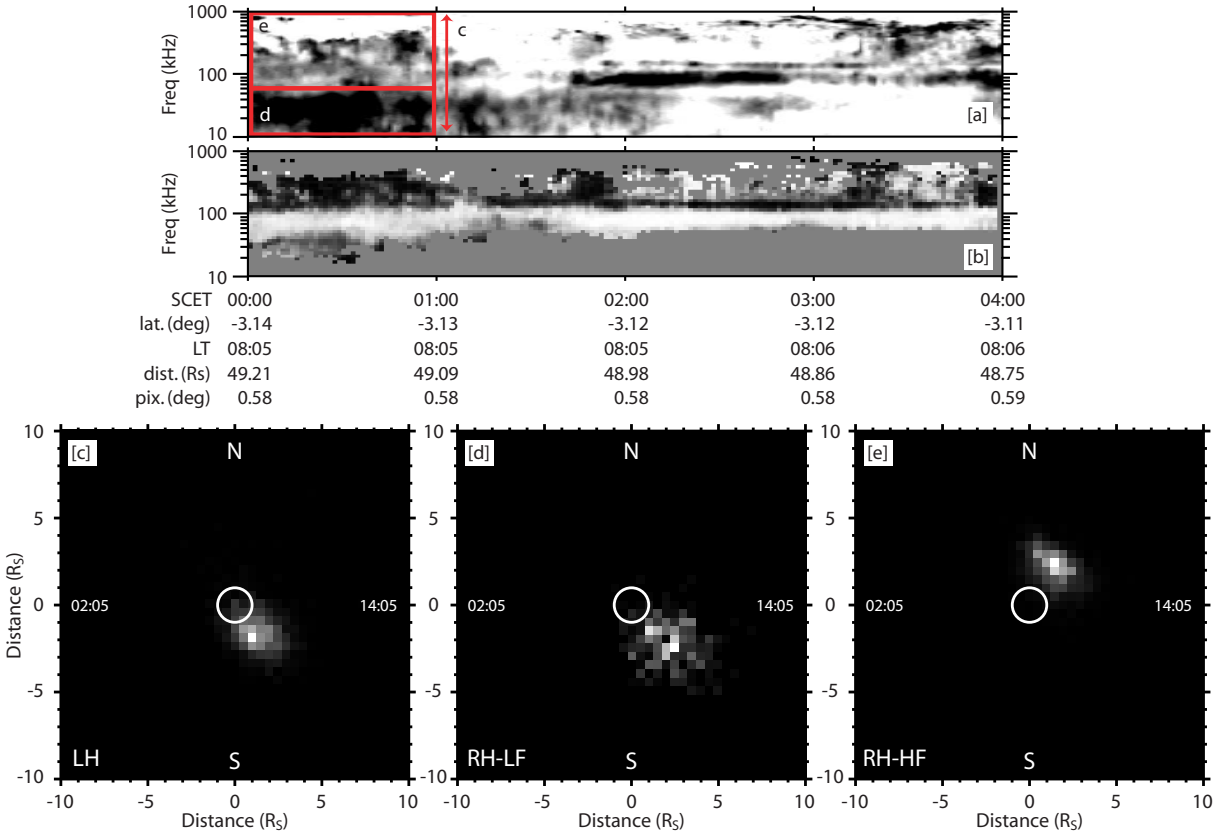

Figure 3: Direction Finding results for day 2005-040. (a) Flux dynamic spectrum summarizing all the radio emissions observed between 00:00 and 04:00 SCET, in the 10–1000 kHz band. (b) Polarization measured in for the same time frequency selection (white is LH, black is RH). Spacecraft time (SCET), latitude (lat.), local time (LT), distance to Saturn (dist.) and angular size of one map pixel (pix.) are shown under plot (b). The four lower plots are intensity maps with the selections: 00:00–01:00 SCET, SNR>33dB; $\alpha_{xw}>20°$ for all and (c) $V>0.3$; (d) $f<60$ kHz, $V<-0.3$; (e) $f>60$ kHz, $V<-0.3$. The white circles represent the size of Saturn, each pixel is $0.5R_S \times 0.5R_S$ at Saturn. The maps units are shown in R_S. The northern and southern direction as well as the mean local time at the limbs are shown at the border of each map.

an intense low frequency SKR episode. It is then emitted on the ordinary (O) mode. It is the first time we have observed such an O-mode radio emission at Saturn.

3.2 Nightside close-range observation (day 2005-089)

For this period of time, the Cassini spacecraft is on an outbound orbit trajectory. Fig. 4a shows the dynamic spectrum of the HFR data recorded during this period. The upper hybrid resonance is visible between 00:00 (at ∼100 *kHz*) and 12:00 (at ∼20 *kHz*). Several bursts of SKR are also visible (the first one begins at ∼05:00 SCET). The four red boxes give the time and frequency selections used to compute the four Fig. 4c–f maps. Fig. 4b shows the circular polarization degree. The gap seen in Fig. 4b between ∼11:00 and

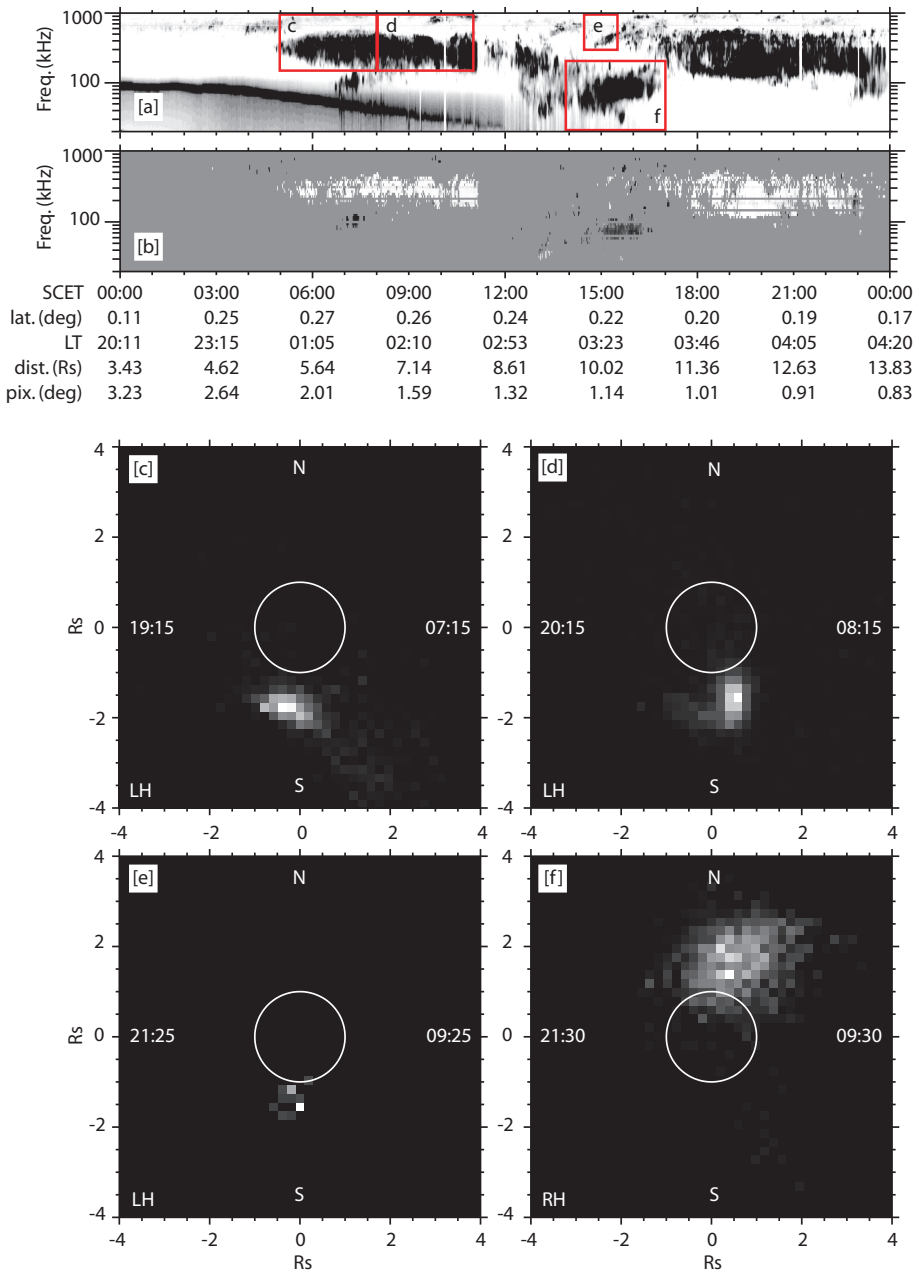

Figure 4: Direction Finding results for day 2005-089. (a) Flux dynamic spectrum summarizing all the radio emissions observed during the day in the 20–1000 kHz band. (b) Polarization measured for the same time frequency selection (white is LH, black is RH). Spacecraft time (SCET), latitude (lat.), local time (LT), distance to Saturn (dist.) and angular size of one map pixel (pix.) are shown under plot (b). The four lower plots are intensity maps with the selections: (c) 05:00–08:00 SCET, f>150 kHz, V>0.3, SNR>33dB; α_{xw}>20°; (d) 08:00–11:00 SCET, f>150 kHz, V>0.3, SNR>33dB; α_{xw}>20°; (e) 14:30–15:30 SCET, f>150 kHz, V>0.3, SNR>33dB; α_{xw}>20°; and (f) 14:00–17:00 SCET, f<150 kHz, V<−0.3, SNR>33dB; α_{xw}>20°. The white circles represent the size of Saturn, each pixel is $0.2R_S \times 0.2R_S$ at Saturn. The maps units are shown in R_S. The northern and southern direction as well as the mean local time at the limbs are shown at the border of each map.

$\sim$13:00 is due to the geometrical selection (α_{xw}>20°) which is needed to get accurate DF measurements.

Cassini is almost in the equatorial plane (its latitude is varying in the 0.1–0.3° range during the studied time interval). The distance to Saturn is increasing from 3.43 to 13.83 R_S. Maps on Fig. 4c–d show the temporal variability of the SKR sources although nothing would indicate such a variability on the dynamic spectrum summary plot (Fig. 4a) or in the circular polarization degree (Fig. 4b). It is also noticeable that the SKR strongly reappears when the Cassini LT position is $\sim$01:00, i.e. when the morning side limb (06:00LT) becomes geometrically visible. Fig. 4c shows a region of emission at high latitude, at $\sim$2.0 R_S, but rather on the dusk side. Fig. 4d shows a region of emission at high latitude, at $\sim$1.7 R_S, on the dawn side. Maps on Fig. 4e–f show an example when both northern and southern SKR sources are visible at the same time. Fig. 4e shows a region of emission at very high latitude and high frequency, at $\sim$1.5 R_S. Fig. 4f shows a strong northern low frequency RH SKR burst, expanding from $\sim$1.2 to $\sim$3 R_S, on the dawn side.

Except for Fig. 4e, the spread of the cloud of points on those figures are larger than the uncertainty on the the DF measurements (1–2°). But as these maps involve time and frequency integration, it is not a measurement of the instantaneous spread of the source, but rather the typical region where the sources are located within the time-frequency selected boundaries.

4 Discussion

We have shown in this paper the first DF results using the Cassini/RPWS/HFR data for the main kronian radio emission, the SKR. We have shown in section 2 that the SKR is strongly circularly polarized: we have measured a 0.87±0.07 degree of circular polarization and no linear polarization has been detected. This result is to be compared to the results given by Ortega-Molina and Lecacheux [1990]. In that study, an indirect method was used to show that a 100% polarization degree was compatible with the measured data and the geometrical configuration of the Voyager-PRA antennas with respect to Saturn. Our *polarimeter inversion* provides the real circular polarization degree as the antenna has already been calibrated. As the Voyager-PRA radio receiver was not providing cross-correlation measurements, Ortega-Molina and Lecacheux [1990] had to calibrate the effective electrical antenna directions using the same data used to derive the polarization. Assuming a 100% circular polarization, they deduced an angle of 82° between Voyager's electrical antennas. From their Fig. 10, our value of V$\sim$90% would imply an angle $\sim$10° smaller.

We have observed that the SKR has no detectable linear polarization degree. This allows us to use the *circular goniometer inversion*. Such results were presented in section 3. The SKR sources localization is compatible with the former studies [see Galopeau et al., 1995; Zarka, 1998]: it is observed at high latitude, in an altitude range which is compatible with the CMI emission process. Measurements on the day side show sources near noon as already inferred through the Voyager-PRA data. Measurements near perikrone and on

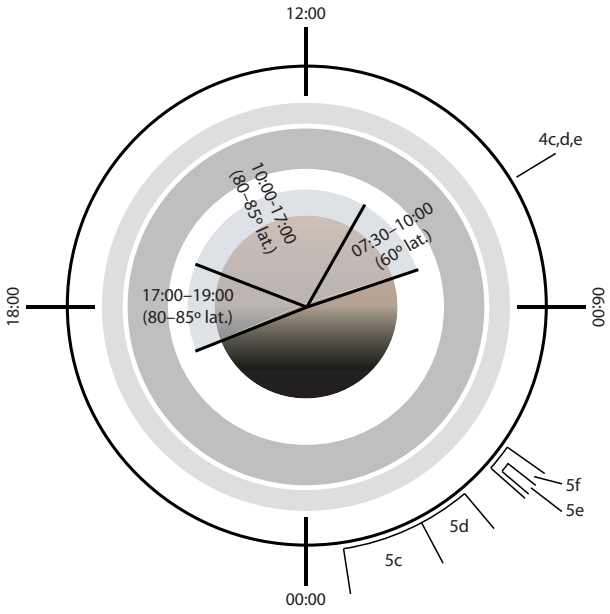

Figure 5: LT position of Cassini for each presented localization results. The grey sectors represent the main emission regions (with respective LT and latitudinal extent) as discussed in Galopeau et al. [1995]. Labels refer to figure numbers.

the night side, show that we observe night side SKR source. Direction Finding shows that the source might be either on the dawn side or on the dusk side. We observe that LH emissions come from the southern hemisphere and RH ones from the northern one. This is fully compatible with CMI emission on the X-mode. We have also observed possible O-mode emission (RH in the southern hemisphere).

Figure 5 summarizes our localization results, showing the position of Cassini corresponding to Fig. 3 and 4, as well as the LT and latitudinal extent of the emission regions inferred from the Voyager-PRA data [Galopeau et al., 1995]: morning source at 07:30–10:00 LT (60° lat.), noon source about 10:00–17:00 LT (80–87° lat.), and evening source at 17:00–19:00 LT ((80–85° lat.). With an emission beaming at ∼70–80° from the magnetic field vector direction at the source, our observations on day 2005-040 are interpreted as follows: Fig. 3c, southern X-mode "noon" source; Fig. 3d, southern O-mode "noon" source; Fig. 3e, northern X-mode "noon" source. The interpretation for observations on day 2005-089 are not as straightforward. Fig. 4d-f are approximately compatible with X-mode morning sources: Fig. 4d, southern morning source; Fig. 4e, high latitude southern (morning?) source; Fig. 4e, high latitude northern morning source. Fig. 4c, however, is compatible neither with a morning source nor with an evening one, as the beaming angle should be ≥90° in both cases. But it could be compatible with the "Radio horizon" model proposed by Lecacheux [2005] (see also [Farrell et al., 2005]) where the radio waves undergo strong propagation effect at or over the planet's limb.

As stated in several studies [Kaiser and Desch, 1984; Genova, 1987], the SKR shows a very Earth-like phenomenology (frequency band, polarization, influence of the solar wind, magnetic moment intensity of the planet, magnetic latitude of the active field lines). Recent high resolution observations with the Wideband Receiver of the RPWS, showed

that the fine structure of the SKR is very close to the one of the AKR and close to the one of jovian decametric emission (DAM) [Kurth et al., 2005b], showing very narrowband tones drifting in time which are interpreted as highly nonlinear processes occurring in the regions of emission. The observation of an O-mode emission in the SKR radio spectrum adds one more similarity between the Earth's and Saturn's radio emission phenomenology.

The results presented in this paper are a first selection of the data and are integrated over one to several hours. They will be completed by more refined analysis including DF studies on smaller time and frequency scales, determination of the L-shell of the SKR source regions, short and long term variability of the SKR sources localization, flux characterization of the emission (beaming, flux, sporadicity).

References

Cecconi, B., and P. Zarka, Direction finding and antenna calibration through analytical inversion of radio measurements performed using a system of 2 or 3 electric dipole antennas, *Radio Science*, **40**, RS3003, 2005.

Connerney, J. E. P., L. Davis, Jr., and D. L. Chenette, Magnetic field models, in *Saturn*, edited by T. Gehrels and M. Matthews, Univ. of Arizona Press, Tucson, 354–377, 1984.

Cowley, S. W. H., E. J. Bunce, and R. Prangé, Saturn's polar ionospheric flows and their relation to the main auroral oval. *Ann. Geophys.*, **22**, 1379–1394, 2004.

De Feraudy, H., A. Bahnsen, and M. Jespersen, Observations of nightside and dayside auroral kilometric radiation with Viking, in *Planetary Radio Emissions II*, edited by H. O. Rucker, S. J. Bauer, and B. M. Pedersen, Austrian Academy of Sciences Press, Vienna, 41–60, 1988.

Farrell, W. M., M. D. Desch, M. L. Kaiser, A. Lecacheux, W. S. Kurth, D. A. Gurnett, B. Cecconi, P. Zarka, A nightside Source of Saturn's Kilometric Radiation: Evidence for an inner magnetosphere energy driver. *J. Geophys. Res.*, **??**, in press, 2005.

Galopeau, P. H. M., P. Zarka, and D. Le Quéau, Source location of Saturn's kilometric radiation: The Kelvin–Helmholtz instability hypothesis. *J. Geophys. Res.*, **100**, 26397–26410, 1995.

Gérard, J.-C., V. Dols, D. Grodent, J. H. Waite, G. R. Gladstone, and R. Prangé, Simultaneous observations of the Saturnian aurora and polar haze with the HST/FOC. *J. Geophys. Res.*, **22**, 2685–2688, 1995.

Gérard, J.-C., D. Grodent, J. Gustin, A. Saglam, J. T. Clarke, and J. T. Trauger, Characteristics of Saturn's FUV aurora observed with the Space Telescope Imaging Spectrograph. *J. Geophys. Res.*, **109**, A09207, doi:10.1029/2004JA010513, 2004.

Gurnett, D. A., W. S. Kurth, D. L. Kirchner, G. B. Hospodarsky, T. F. Averkamp, P. Zarka, A. Lecacheux, R. Manning, A. Roux, P. Canu, N. Cornilleau-Wehrlin, P. Galopeau, A. Meyer, R. Boström, G. Gustafsson, J.-E. Wahlund, L. Ahlen, H. O.

Rucker, H. P. Ladreiter, W. Macher, L. J. C. Woolliscroft, H. Alleyne, M. L. Kaiser, M. D. Desch, W. M. Farrell, C. C. Harvey, P. Louarn, P. J. Kellogg, K. Goetz, and A. Pedersen, The Cassini Radio and Plasma Wave investigation, *Space Sci. Rev.*, **114**, 1, 395–463, 2004.

Kaiser, M. L., M. D. Desch, J. W. Warwick, and J. B. Pearce, Voyager Detection of Nonthermal Radio Emission from Saturn. *Science*, **209**, 1238–1240, 1980.

Kaiser, M. L., and M. D. Desch, Radio emissions from the planets Earth, Jupiter and Saturn. *Rev. Geophys. Space Phys.*, **22**, 373–384, 1984.

Kurth, W. S., D. A. Gurnett, J. T. Clarke, P. Zarka, M. D. Desch, M. L. Kaiser, B. Cecconi, A. Lecacheux, W. M. Farrell, P. Galopeau, J.-C. Gérard, D. Grodent, R. Prangé, M. K. Dougherty, and F. J. Crary, An Earth-like correspondence between Saturn's auroral features and radio emission. *Nature*, **433**, 722–725, doi:10.1038/nature03334, 2005a.

Kurth, W. S., G. B. Hospodarsky, D. A. Gurnett, B. Cecconi, P. Louarn, A. Lecacheux, P. Zarka, H. O. Rucker, M. Boudjada, and M. L. Kaiser. High Spectral and Temporal Resolution Observations of Saturn Kilometric Radiation. *Geophys. Res. Lett.*, **32**, L20S07, 2005b..

Lecacheux, A., The "Radio Horizon" effect, as a possible explanation of the planetary, auroral radio emission phenomenology. *Planetary Radio Emission VI Conference*, Austrian Acad. of Science, Graz, Austria, April 2005.

Louarn, P., Auroral planetary radio emissions, theoretical aspects. *Adv. Space Res.*, **8**, 121–134, 1992.

Ortega-Molina, A., and A. Lecacheux, Polarization response of the Voyager-PRA experiment at low frequencies, *Astron. Astrophys.,* **229,** 558, 1990.

Trauger, J. T., J. T. Clarke, G. E. Ballester, R. W. Evans, C. J. Burrows, D. Crisp, J. S., Gallagher, III, R. E. Griffiths, J. J. Hester, J. G. Hoessel, J. A. Holtzmann, J. E. Krist, J. R. Mould, R. Sahai, P. A. Scowen, K. R. Stapelfeldt, and A. M. Watson, Saturn's hydrogen aurora: Wide field and planetary camera 2 imaging from the Hubble Space Telescope, *J. Geophys. Res.*, **103**, 20237–20244, 1998.

Vogl, D. F., B. Cecconi, W. Macher, P. Zarka, H. P. Ladreiter, P. Fédou, A. Lecacheux, T. Averkamp, G. Fischer, H. O. Rucker, D. A. Gurnett, W. S. Kurth, and G. B. Hospodarsky, Inflight calibration of the Cassini-Radio and Plasma Wave Science (RPWS) antenna system for direction-finding and polarization measurements, *J. Geophys. Res.*, **109**, A09S17, doi:10.1029/2003JA010261, 2004.

Zarka, P., Auroral radio emissions at outer planets: Observations and theories. *J. Geophys. Res.*, **103**, 20159–20194, 1998.

Zarka, P., Radio emissions from the planets and their moons, in *Radio Astronomy at Long Wavelengths*, Geophys. Monogr. **119**, edited by R. G. Stone, J.-L. Bougeret, K. Weiler, and M. Goldstein, American Geophysical Union, Washington, 167–178, 2000.